World Journal of Radiology

Online Submissions: http://www.wjgnet.com/1949-8470office
wjr@wjgnet.com
doi:10.4329/wjr.v3.i1.1

World J Radiol 2011 January 28; 3(1): 1-16
ISSN 1949-8470 (online)

EDITORIAL

Multiparametric MRI biomarkers for measuring vascular disrupting effect on cancer

Huaijun Wang, Guy Marchal, Yicheng Ni

Huaijun Wang, Guy Marchal, Yicheng Ni, Department of Radiology, University Hospitals, University of Leuven, Herestraat 49, B-3000 Leuven, Belgium
Author contributions: All authors made a substantial contribution to the conception and design of the manuscript, drafting the article or revising it.
Supported by (partially) The grants awarded by Fonds voor Wetenschappelijk Onderzoek-Vlaanderen (FWO Vlaanderen) Impulsfinanciering project (ZWAP/05/018); Geconcerteerde Onderzoeksactie of the Flemish Government, OT project (OT/06/70); the K.U. Leuven Molecular Small Animal Imaging Center MoSAIC (KUL EF/05/08); the center of excellence In vivo Molecular Imaging Research of K.U. Leuven; and a EU project Asia-Link CfP 2006-EuropeAid/123738/C/ACT/Multi-Proposal No. 128-498/111
Correspondence to: Dr. Yicheng Ni, Professor, Department of Radiology, University Hospitals, University of Leuven, Herestraat 49, B-3000 Leuven, Belgium. yicheng.ni@med.kuleuven.be
Telephone: +32-16-330165 Fax: +32-16-343765
Received: December 7, 2010 Revised: January 13, 2011
Accepted: January 20, 2011
Published online: January 28, 2011

Abstract

Solid malignancies have to develop their own blood supply for their aggressive growth and metastasis; a process known as tumor angiogenesis. Angiogenesis is largely involved in tumor survival, progression and spread, which are known to be significantly attributed to treatment failures. Over the past decades, efforts have been made to understand the difference between normal and tumor vessels. It has been demonstrated that tumor vasculature is structurally immature with chaotic and leaky phenotypes, which provides opportunities for developing novel anticancer strategies. Targeting tumor vasculature is not only a unique therapeutic intervention to starve neoplastic cells, but also enhances the efficacy of conventional cancer treatments. Vascular disrupting agents (VDAs) have been developed to disrupt the already existing neovasculature in actively growing tumors, cause catastrophic vascular shutdown within short time, and induce secondary tumor necrosis. VDAs are cytostatic; they can only inhibit tumor growth, but not eradicate the tumor. This novel drug mechanism has urged us to develop multiparametric imaging biomarkers to monitor early hemodynamic alterations, cellular dysfunctions and metabolic impairments before tumor dimensional changes can be detected. In this article, we review the characteristics of tumor vessels, tubulin-destabilizing mechanisms of VDAs, and *in vivo* effects of the VDAs that have been mostly studied in preclinical studies and clinical trials. We also compare the different tumor models adopted in the preclinical studies on VDAs. Multiparametric imaging biomarkers, mainly diffusion-weighted imaging and dynamic contrast-enhanced imaging from magnetic resonance imaging, are evaluated for their potential as morphological and functional imaging biomarkers for monitoring therapeutic effects of VDAs.

Key words: Vascular disrupting agents; Tumor vessels; Imaging biomarkers; Magnetic resonance imaging; Diffusion-weighted imaging; Dynamic contrast-enhanced magnetic resonance imaging

Peer reviewer: Rivka R Colen, MD, Department of Radiology, Brigham and Womens Hospital, 75 Francis St, Boston, MA 02115, United States

Wang H, Marchal G, Ni Y. Multiparametric MRI biomarkers for measuring vascular disrupting effect on cancer. *World J Radiol* 2011; 3(1): 1-16 Available from: URL: http://www.wjgnet.com/1949-8470/full/v3/i1/1.htm DOI: http://dx.doi.org/10.4329/wjr.v3.i1.1

INTRODUCTION

For non-surgical anticancer strategies such as conventional radiotherapy and chemotherapy, the main disadvantage is lacking specificity for cancer tissue, i.e. concomitant

cytotoxic effects on normal tissues. In order to find more selective treatments, researchers have made efforts to exploit morphological, physiological and microenvironmental differences between normal and malignant tissues, including microvasculature, oxygenation and necrosis. One of the most prominent differences lies in the tumor neovasculature[1].

Tumor vasculature is a crucial component of pathophysiology in solid tumors, which affects growth, metastasis and therefore, response to therapy. Compared with the normal vasculature, tumor vessels are less mature in structure and leakier, where blood flow is spatially and temporally heterogeneous and often compromised. Furthermore, hyperpermeability of the vascular wall and lack of functional lymphatics within tumors elevate interstitial fluid pressure in solid tumors[2,3]. The molecular mechanisms of abnormal tumor vasculature may result from the imbalance between pro- and antiangiogenic regulating factors in tumor as well as host stromal cells[4]. Such vascular characteristics of solid tumors are sufficiently different from those of normal tissues and thus provide a unique target for tumor treatment[1].

Drugs developed for vascular targeting therapies can be divided into two different groups: antiangiogenic agents for inhibiting the formation of new vessels and vascular disrupting agents (VDAs) for destroying the existing vessels[5]. Hallmark characteristics with VDAs are selective reduction in tumor blood flow, induction of ischemic tumor necrosis, presence of viable neoplastic cells at the tumor periphery, and effect on delaying tumor growth[6]. According to their action mechanisms, VDAs can be further categorized into ligand-directed VDAs and small molecule VDAs. Small molecule VDAs include flavonoids such as 5,6-dimethylxanthenone-4-acetic acid (DMXAA/ASA404), and tubulin-destabilizing agents[7]. As a tubulin-destabilizing VDA, c*is*-1-(3,4,5,-trimethoxyphenyl)-2-(4'-methoxyphenyl)ethene-3'-0-phosphate or combretastatin A-4-phosphate (CA4P/Oxi2021) is most representative, and has been under phase Ⅲ clinical trials.

Unlike other conventional chemotherapies, VDAs are cytostatic rather than cytotoxic to malignant cells. They starve and indirectly kill tumor cells by depleting their blood supply, and can only delay tumor growth but not eradicate the tumor. Given this novel action mechanism, imaging biomarkers have been elaborated to detect and quantify non-invasively VDA-induced morphological, functional and metabolic alterations. Relative to the conventional clinical endpoints such as mortality and morbidity, these imaging biomarkers work in a more prompt, predictable and precise way[8,9]. Hereby, the term biomarker is adopted more broadly than its traditional definition, i.e. a biomarker can be derived not only from biofluid samples with the techniques of biochemistry and molecular biology, but also from modern imaging metrics including magnetic resonance imaging (MRI), computed tomography (CT), positron emission tomography (PET) or single photon emission tomography (SPECT), ultrasound, and optical imaging[10]. In this article, we review the action mechanisms of tubulin-destabilizing VDAs and the preclinical and clinical results of two lead VDAs, CA4P and ZD6126 (N-acetylcolchinol-O-phosphate), with the emphasis on the role of MRI in the preclinical evaluation of VDA effects.

VDAs

Pathophysiological features of tumor vessels as targets of VDAs

Oxygen diffusion distance from capillaries is only 150-200 μm. Because of the unrestrained growth, tumor cells growing outwith this effective diffusion distance become hypoxic and eventually necrotic[11-13]. Therefore, a tumor has to develop its own vessels to maintain its growth, i.e. angiogenesis, when its diameter exceeds about 0.5 mm[14].

These newly developed tumor vessels are often immature: the endothelial cells are irregular-shaped with larger interendothelial conjunctions[15,16] and poor connections between the endothelial lining and irregular basement membrane[17,18]. Due to these characteristics, tumor vessels are hyperpermeable and interstitial fluid pressure is higher than in normal tissues. Such high pressure is also contributed by the inefficient drainage with dysfunctional tumor lymphatics, which can be caused by rapid proliferation of tumor cells in a confined space, which creates mechanical stress that compresses intratumor lymphatics[19,20]. Besides, malignant tumors are known to feature with lymphatic deficiency or retarded development of lymphatics[19,20]. Tumor vessels are tortuous, disorganized and non-hierarchical, with complex branching of heterogeneous length and diameters, leading to high resistance to perfusion[21]. Under such conditions, any slight fluctuation of blood perfusion may cause catastrophic events in tumor vessels, while it has little effect on normal tissue, because mature vessels are more robust against perfusion changes due to efficient regulating mechanisms[21].

Role of cytoskeleton in the regulation of endothelial barrier function

The endothelial barrier keeps the blood cells from exposure to surrounding tissues. Endothelial cells (ECs) line the inner surface of blood vessels and rely on their cytoskeleton to maintain the structural integrity of confluent monolayer and flat shape. Dysfunction in cellular shape can cause subsequent vascular hyperpermeability[22]. The cytoskeleton consists of three distinct components: microtubules, actin microfilaments and intermediate filaments[23], and the former two are associated *via* linking proteins, which, in turn, interact with these two cytoskeletal components for signaling[24]. As the scaffolding of the cell, the cytoskeleton plays a vital role in cell motility, division, shape maintenance, and signal transduction[24]. In tumor vessels, actin is ill-developed and thus the maintenance of cell shape depends more on microtubules[25,26].

The delicate dynamic balance between the centripetal tension and centrifugal force to ensure the cellular shape is finely modified by cytoskeleton and intercellular junc-

tional complexes of membrane-binding proteins that provide intercellular adherence, which is regulated by several signaling pathways[22]. Reorganization of actin leads to the assembly of bundled stress fibers, and therefore, increased cellular contractility. The main constituent of intercellular junctions is vascular endothelial (VE) cadherin/β-catenin complex anchored to actin[22]. Disruption of the VE-cadherin/β-catenin pathway causes the loss of intercellular junctional organization, dysfunction of monolayer barrier, and eventual rounding up of ECs[27].

Mechanisms of VDA action

The mechanisms of action with VDAs still need to be fully elucidated. It has been speculated that CA4P binds to tubulin of microtubule at or close to the colchicine-binding site[28]. Unlike the antitumor effect with colchicine that is only achievable at a dose close to the maximum tolerated dose (MTD), the effect with VDAs is observed within a wide therapeutic window lower than the MTD. Their ability to selectively target the cytoskeleton and compromise the endothelial intercellular junctions is vital to their mechanisms of action[7]. CA4P has been most extensively studied. Therefore, we take CA4P as an example to discuss the potential molecular and cellular mechanisms of action, which are likely to be applicable to other tubulin-binding VDAs such as ZD6126.

On a long-term basis, CA4P inhibits the microtubule dynamics, interferes with the mitotic spindle function and leads to cell cycle arrest, which results in proliferation blockage and/or apoptosis[29]. Although such a direct cytotoxic or antiproliferative effect may contribute to the antivascular effects of CA4P, it would be too slow to account for the rapid vascular shutdown observed *in vivo*, which can occur within minutes after CA4P treatment in animal models[30]. Rather, immediate morphological and functional changes are more likely to be involved in such vascular collapse.

In vitro, it has been shown that Rho-GTPase plays an important role in the capillary-like collapse (Figure 1). Belonging to signaling G protein (GTPase), Rho proteins (Ras homologous proteins) are interconnected with microtubules[31]. The members of the Rho-GTPase family are essential in converting and amplifying external signals into cellular effects, including regulation of actin dynamics and cadherin/β-catenin pathway[32,33].

CA4P selectively binds to microtubules and depolymerizes tubulin, which results in the activation of Rho-GTPase and its associated Rho kinase[34-36] (Figure 1). Activation of the Rho/Rho-kinase pathway may cause downstream morphological and/or functional changes in ECs, which can lead to dysmorphism and hyperpermeability: (1) assembly of actin stress fibers and fortified contractility of ECs[24]; (2) disruption of the VE-cadherin/β-catenin complex to induce the loss of intercellular adhesion and the appearance of paracellular gaps[22]; (3) blebbing of ECs with regulation of stress-activated protein kinase p38 (SAPK-2/p38) to bring about increased monolayer permeability and resistance to blood flow[36,37]; and (4) vasoconstriction to give rise to increased geometric resistance to blood flow[38]. In addition, the direct binding of CA4P to tubulin compromises the integrity of cytoskeleton, and morphological changes of endothelial monolayer architecture further deteriorates[7,39] (Figure 1).

With the increased vascular permeability, the consequent leakage of plasma macromolecule into extravascular extracellular space (EES) results in fluid loss, increased hematocrit and formation of rouleaux[40]. As a result, the resistance to blood flow is increased. After EC damage, direct exposure of basement membrane to flowing blood initiates coagulation and hemorrhage[40]. Accordingly, the drop in blood flow induces hypoxia and deprivation of nutrients and subsequent necrosis of tumor (Figure 1).

In vivo, the increase in permeability may be the key event responsible for the VDA-induced vascular collapse[41]. Although the primary effects of CA4P have been confirmed *in vivo*, including morphological changes in ECs, such as blebbing[42] and increased permeability and vasoconstriction in arterioles[38], direct evidence of mechanisms *via* the activation of Rho/Rho-kinase pathway are still sparse. However, the CA4P-induced vascular shutdown effect is attenuated in combination with Rho or Rho kinase inhibitors[7,36,43], while amplified in combination with an anti-VE-cadherin agent[44], which may be considered indirect proof of the link between the cytoskeletal remodeling and permeability.

Dose of VDAs

Some VDAs are orally active, e.g. ABT-751[39] and CYT 997[45], while intraperitoneal (ip) and intravenous (iv) administrations are most frequently applied in the treatment of tumors in rodent models. The ip injection is convenient for the handing of rodents, while it fails to mimic the clinical practice where iv injection is applied. Successful iv injection ensures an effective dose of VDA in the systemic circulation.

For single doses of CA4P, the MTD is estimated to be around 68 mg/m^2 in patients[46], which gives the clinically relevant dose of about 10 mg/kg in rats[47,48]. In mice, the roughly estimated MTD is 1000-1500 mg/kg[49]. However, the lowest effective dose is 25 mg/kg, which is already higher than the MTD in humans. Therefore, the CA4P effect with higher doses in mice is difficult to translate into humans[50].

For single doses of ZD6126, the MTD in patients is about 112 mg/m^2, which gives the clinically relevant dose of about 10 mg/kg in rats[51]. In mice, the MTD is about 750 mg/kg[52].

The tumor response to various VDAs depends mainly on drug type, tumor model and dosing regimen in preclinical studies. Generally speaking, the higher dose of VDAs can induce more striking antivascular effect, while the results cannot be convincingly translated into clinical practice if the dose for animal models exceeds the MTD in patients. Therefore, the results with clinically relevant doses in tumor models may better predict the outcomes in patients.

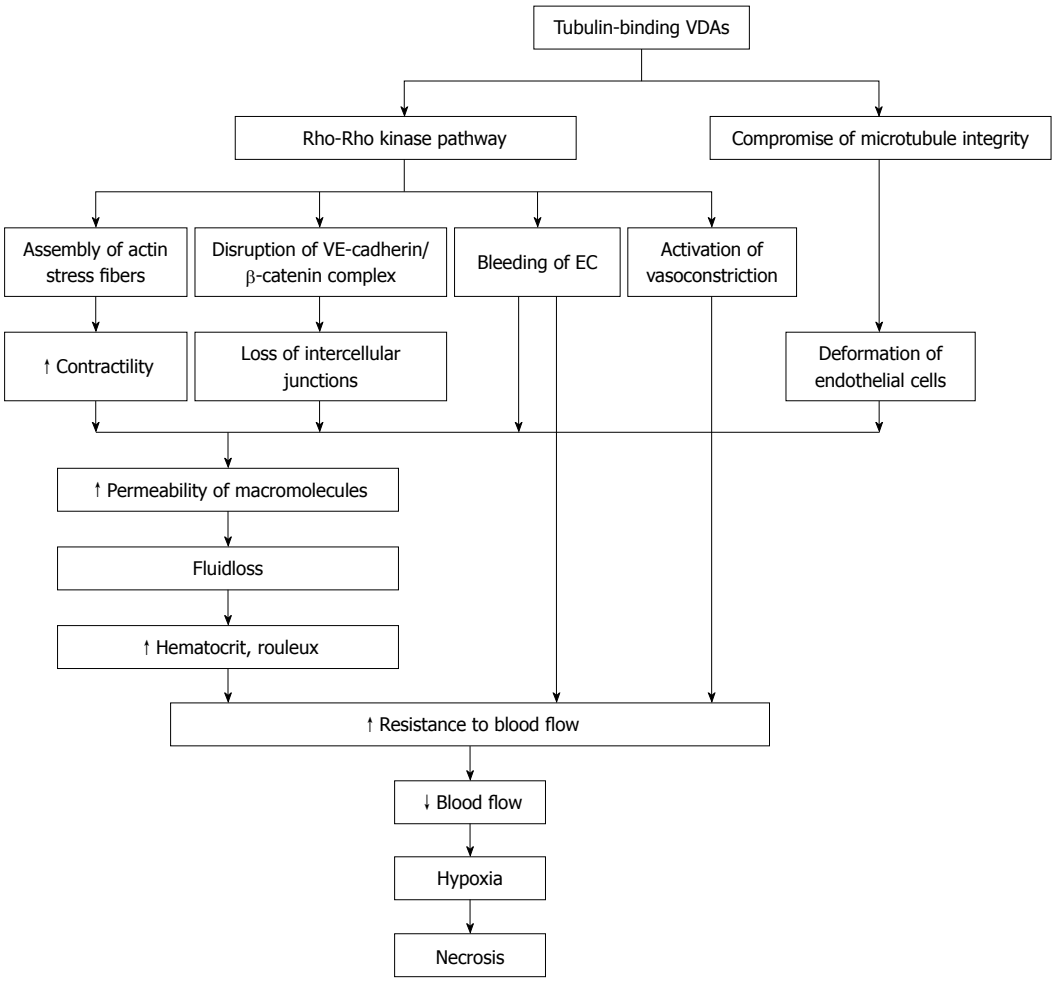

Figure 1 Schematic mechanisms of action with tubulin-binding vascular disrupting agents. VE: Vascular endothelial; VDAs: Vascular disrupting agents; EC: Endothelial cell.

In vivo effect

After VDA treatment, a rapid increase in tumor vascular permeability triggers the catastrophic cascade of vessel collapse *in vivo*. A decrease in blood flow occurs almost immediately, and reaches the maximum in the following several hours. The collapsed blood supply induces central necrosis of the tumor. However, tumor sparing still exists at the periphery, leading to relapse after single-dose treatment[53-56]. The efficacy of such therapy relies largely on how fast blood supply is recovered. This restoration is unavoidable, because the tumor cells at the periphery can obtain a direct supply of oxygen and nutrients from neighboring normal tissues and engulfed normal vessels during the fast growth of malignancies[7,56]. Thus, growth of the tumor is only delayed due to the compromised blood supply and it cannot be eradicated.

Histopathologically, VDA-induced necrosis is located in the center of the tumor with a characteristic viable rim of a few cell layers adjacent to the normal tissue surrounding the tumor mass, which persists irrespective of differences in potency and efficacy of VDAs. In addition, hemorrhage often occurs together with necrotic tumor cells several hours after treatment[57]. Besides, the infiltration by inflammatory leukocytes may also contribute to the vascular-disrupting effect[41,42].

After VDA treatment, tumors may become phenotypically more aggressive due to hypoxia. With the regulation of hypoxia inducible factor 1α (HIF-1α), expression of angiogenic gene is activated and the level of vascular endothelial growth factor (VEGF) is thus increased[55,58]. Therefore, antiangiogenic therapy may be complementary to VDA, providing dual targeting at both preexisting and new vessels.

ANIMAL TUMOR MODELS

In vivo cancer research in clinically relevant animal models bridges the *in vitro* studies of cell culture and biochemical assays with the more costly, time-consuming clinical practice. Considering the greater costs and stricter ethical regulations on human studies, a variety of rodent tumor models have been introduced particularly in combination with multiparametric imaging biomarkers to envisage the internal real-life events in experimental VDA research.

These animal models with various tumor cell lines can be classified according to several features. For examples, they can be categorized by locations such as subcutaneous[51,59], intramuscular[60-62] or visceral organ[57] tumors; by destination relative to source graft such as orthotopic[63-65] or ectopic tumors; by carcinogenesis such

as primary[26,48,65,66] or secondary tumors; by graft origins such as allograft[63] or xenograft human[61,67,68] or animal[69] tumors; and by immune status of tumor recipient such as the tumors growing in immunocompetent or immunodeficient[64,68] animals.

A wide range of diverse VDA effects have been observed in various tumor models[70,71]. Tumor microenvironment and host-tumor interaction may account for such discrepancy in responsiveness. Besides tumor cells with gene mutations, host stromal cells are also greatly involved in the tumor initiation, progression, invasion, and metastasis. For instance, with the expression of VEGF, stromal fibroblasts play a role in the formation and maintenance of tumor vessels[2]. Accordingly, when transplanted into various host locations or organs, the same neoplastic graft may have different angiogenesis and vascular functions. Thus, response to the same treatment may differ depending on tumor location and host-tumor interaction, because the organ-specific regulation of the balance between pro- and anti-angiogenic factors is responsible for the different angiogenesis activities[2,4,62,72]. As a result, tumor models of orthotopic transplantation into visceral organs of host animals with intact immune functions are thought to be more relevant to the conditions of clinical patients in terms of better mimicking tumor microenvironment, therefore, the treatment outcomes are more translatable into patients[62,72].

For imaging studies of VDA effects in small rodents, image quality has been shown to be satisfactory, even for organs susceptible to motion artifacts with non-respiratory-gated acquisition at a clinical magnet[56]. However, imaging in mice is more challenging than in rats, because the body weight of a mouse is about one-tenth of a rat, which results in lower signal-noise ratio (SNR) and poorer spatial resolution. In addition, success rate is sometimes compromised for the repetitive cannulations for intravenous injection of VDAs or contrast agents in mice during the dynamic follow-up of treatment monitoring, leading to some missing data.

MEASURING TUMOR RESPONSE TO VDAs WITH *IN VIVO* IMAGING BIOMARKERS

VDAs have been shown to induce vascular shutdown in tumors within minutes, and how to evaluate accurately and promptly such effects remains a challenge to preclinical research and clinical practice. Ineffective treatment may not only hamper or delay the effective alternative therapies, but also cause unnecessary side effects and waste of resources. Considering the presence of possible non-responders to certain therapies, it is of immense importance to individualize the treatment regimens, in which early feedback after VDA treatment is deemed crucial.

For the assessment of anticancer effects, traditional clinical endpoints are difficult to quantify and may require lengthy and larger scales to complete[8,9]. Thus, it is impractical to perform such endpoints in the assessment of early effects with VDAs. Recently, multiparametric imaging biomarkers have been developed as "surrogate endpoints" to act as indispensable substitutes for such clinical endpoints. The quantitative structural, functional and metabolic information derived from these imaging biomarkers may enable more comprehensive assessments and predictions of clinical outcomes, and in this case, the possibility for timely therapeutic justification and adjustment in oncological patients under the VDA regimen.

Out of various imaging modalities, MRI has been most frequently applied for the evaluation of VDA effects due to its advantages such as excellent spatial and temporal resolution, imaging in arbitrary planes, no ionizing radiation and ability to provide morphological, functional and metabolic information (with MR spectroscopy) for serial post-treatment follow-up. In the following section, we focus on the role of MRI in the evaluation of VDAs and its validation with other robust and specific techniques.

Clinical and high-field-strength MRI scanners

For preclinical research and clinical trials of VDAs, some animal studies have been performed with clinical 1.5 T MRI scanners[56,59,73], and more studies on small-bore research scanners[51,53,62,64,68,69,74,75]. The clinical and animal scanners are different in terms of availability in research centers, accessibility during working hours, usability, difficulty in method development, and translatability. Most important, with some parametrical optimization of built-in sequences, clinical scanners yield more translational results from small rodents to clinical patients than do dedicated animal scanners.

Recently, 3.0 T clinical scanners have become widely available with a trend for introducing even higher field whole body scanners (7-11 T) throughout the industry, since the safety approval of 3.0 T scanners in patients in 2002[76]. For intracranial tumors, 3.0 T scanners have shown better SNR, spatial and temporal resolution, contrast-to-noise ratio, and spectral resolution than 1.5 T scanners with the same acquisition parameters[76-79]. However, the applications in other regions of the body, the added value of 3.0 T compared with 1.5 T scanners is still controversial, due to issues such as specific absorption rate and motion and susceptibility artifacts. The modification of acquisition parameters and development of new coils may lead to wider applications in body imaging with 3.0 T MRI[80,81].

Biomarkers from conventional MRI sequences

Conventional MRI biomarkers are derived from T2-weighted imaging (T2WI), T1-weighted imaging (T1WI) and contrast-enhanced T1WI (CE-T1WI). Despite the topographic information such as tumor location, shape and volume, the quantification of tumor signal intensity (SI) on T2WI can help to detect VDA-induced hemorrhage[64]. SI on T2WI can also help to differentiate the viable tissue from necrosis on a pixel-based image texture analysis[82]. The heterogeneous SI on T2WI after VDA

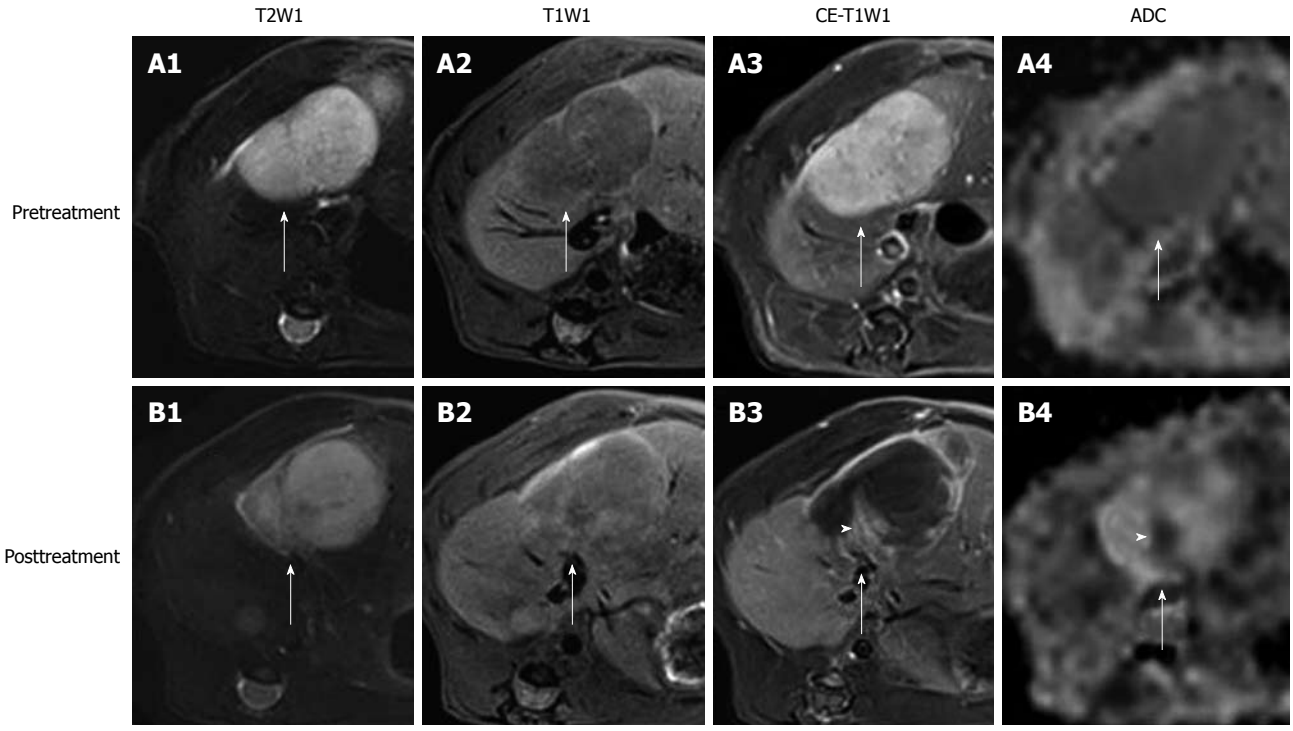

Figure 2 ***In vivo*** **magnetic resonance imaging findings of an implanted tumor in rat liver.** Before treatment, the tumor (arrows) appeared hyperintense on T2WI (A1); hypointense on T1WI (A2); strongly enhanced on CE-T1WI (A3); and slightly hypointense on ADC_{high} (b = 500, 750, 1000 s/mm^2) (A4). At 24 h after the intravenous treatment with CA4P at 10 mg/kg, obvious vascular shutdown was observed. The tumor (arrows) was still hyperintense on T2WI (B1) and hypointense on T1WI (B2). On CE-T1WI, the tumor (arrow) appeared hypointense in the center with an enhanced rim of viable neoplastic cells (B3). On ADC_{high} map (B4), the hyperintensity in the center corresponded to necrosis, and the isointense ring was concordant with the viable tumor rim (arrow) on CE-T1WI. Note the viable tumor nodule at the periphery, shown as hyperintensity (arrowhead) on CE-T1WI (B3), and hypointensity (arrowhead) on ADC_{high} (B4).

treatment is associated with (hemorrhagic) necrosis and complicated by evolving stages of necrosis and/or deoxyhemoglobin. Accordingly, SI change in T2WI is not considered a consistent imaging biomarker of hemorrhagic necrosis[51,71].

To date, the most frequently used surrogate endpoint for therapeutic evaluation of tumor response is the change in tumor size[83]. Tumor size can be measured linearly with 1D or 2D longest axis, although it may often lead to the overestimation of tumor volume of irregular shape. Manual delineation of tumor in tumor-containing slices or computer-assisted 3D analysis is more accurate for the estimation of tumor volume. Tumor volume of 3D analysis is predictive of survival in patients with tumors[84,85]. However, the change in tumor size/volume always falls as a late event behind the earlier and complex changes in microstructure and function induced by the downstream molecular and cellular events after VDA treatment[42,57], because VDAs only slow down the tumor growth without tumor eradication or size reduction[86]. Therefore, tumor size/volume is not a suitable imaging biomarker for very early assessment of the outcomes with VDAs (Figure 2).

Enhancement ratio is defined as the enhancement degree of tumor post-treatment on CE-T1WI relative to that before treatment[56]. It largely reflects the proportional distribution of contrast agent in blood vessels and EES of viable tumor tissues, and can be used for roughly assessing tumor vascularity, but it lacks the specific physiological meaning (Figure 2).

The necrosis ratio as an imaging biomarker for the evaluation of anticancer therapy has been endorsed as well as tumor size by the European Association for the Study of the Liver and the American Association for the Study of Liver Diseases[87,88]. The necrosis ratio can be measured on CE-T1WI, exploiting the perfusion deficit caused by the vascular shutdown in the non-viable tumor tissue (Figure 2). However, in this way, the necrosis ratio with non-specific contrast agent is underestimated due to inward diffusion of the contrast agent from the viable rim to the necrotic center of the tumor, when correlated with the necrosis ratio measured by histopathology[56,89]. Another method is to delineate the necrotic part on dynamic contrast-enhanced MRI (DCE-MRI) in order to minimize the diffusion of contrast agent[90]. Nevertheless, DCE-MRI has a relatively poor spatial resolution despite its high temporal resolution, i.e. the viable and necrotic tumor is sometimes difficult to discern on DCE-MRI. It needs to be explored which way to determine necrosis ratio can correlate better with the histopathological results. As an alternative to histopathology, the necrosis ratio from MRI may provide an imaging tool for assessing necrosis for the serial follow-up of patients after reliable necrosis develops. The ultimately reliable determination of necrosis may only be realized with the use of necrosis-avid contrast agents, which are not clinically available[91,92].

Conventional MRI biomarkers are easier to acquire and analyze, while they only reveal incomplete pathophysiological processes, and are often too late compared with

very rapid shutdown after VDA treatment. Thus, it is imperative to develop more prompt, accurate, quantifiable, and specific imaging biomarkers for characterizing those early molecular and cellular changes, which can be clinically applicable to depicting early functional and metabolic changes, offering the insight into VDA mechanisms of action, dictating the course of therapy, and predicting treatment outcomes. Fortunately, the recent rapid advances in MRI and other modalities have made such requirements feasible for developing functional imaging biomarkers.

Diffusion-weighted imaging

First applied in neuroimaging, diffusion-weighted imaging (DWI) has rapidly evolved into a non-invasive oncological tool in the body, including the brain[93,94]. As a quantitative functional biomarker for detection and characterization of tumor, DWI is easy-to-perform and contrast-agent-free, and its innate imaging contrast is not significantly affected by exogenous contrast agents[95,96]. Therefore, DWI can be applied in patients with renal dysfunction, where contrast agents are contradicted, for repetitive monitoring after VDA treatment[97,98].

Basic principles: At a microscopic level, all water molecules undergo thermally driven random movement in three dimensions, so-called Brownian motion. Diffusion is a measure for the effective moving distance of water molecules within a given time[99,100]. In biological tissue, the mobility of water molecules are unavoidably hampered by their interaction with cell membranes, intracellular organelles and macromolecules, so that their apparent diffusion coefficient (ADC) within tissues in physiological or pathological conditions is determined by tissue cellularity, tissue components, and tortuosity of EES[101,102]. On the other hand, ADC is also affected by microscopic flow due to microcirculation within a voxel and water exchange between intracellular and extracellular compartments[8,103]. In general, ADC reflects the information of cellular density and membrane integrity, as well as different weighting of perfusion components, depending on the various diffusion gradients applied in the acquisition[103].

DWI can be obtained by applying two symmetrical diffusion-sensitizing gradients on the either side of a 180° refocusing pulse to a T2-weighted sequence. In a DWI sequence, moving water molecules undergo a phase shift after the first diffusion gradient and their phase shift cannot be canceled out as for static molecules after the second gradient, which causes the signal loss of moving water molecules on DWI. The imaging contrast between mobility-restricted and normal water molecules is thus created on SI[99]. For example, tumor tissues normally have higher cellular density, and after VDA treatment, edema with restricted mobility of water and necrosis with elevated diffusion in EES can be differentiated from normal tissues on DWI[86,104]. A diffusion gradient is characterized by the amplitude, duration and direction of diffusion-sensitizing factor (b value with the units s/mm^2), and the weighting of diffusion on SI depends on b value[99]. For quantification of ADC, gradients are applied in three directions (X, Y and Z axes). However, in tissues in which mobility of water molecules is restricted by some structural barriers such as fiber bundles in the brain, diffusion anisotropy is quantified in more than six directions on diffusion tensor imaging (DTI)[105].

ADC-Quantification of DWI: Frequently expressed in a unit of 10^{-3} mm^2/s, ADC is more robust against the influence of magnetic field strength and T2 shine-through effect, which facilitates intra- and inter-subject comparisons[106]. ADC can be quantified with the following least-squares algorithm[99]: $ADC = \ln(S_0/S_i)/b_i$ (1), where S_i is the SI measured on the ith b value image and b_i is the corresponding b value. S_0 is a variable that estimates the intrinsic SI (for b = 0 s/mm^2). In tumors, such quantification requires at least two values in one direction, while more than three values are used to reduce noise[107]. ADC value can be generated with mono-exponential fit between SI and b value for each voxel, and displayed as a parametric map for all voxels[94].

It is important to bear in mind that intravoxel incoherent motion (IVIM) may dominate ADC values in biological tissues when lower b values are used. This means that, for a given voxel, not only the diffusion of water molecules contributes to its ADC, but also the microcirculation of blood in capillary within the voxel[103]. In tumors, rapid blood flow leads to non-linearity of ADC fitting within lower range of b values, i.e. small increase in b value causes bigger attenuation of SI[108,109].

For the calculation of ADC, the usual method is to obtain an overall ADC fitting of mono-exponential decay through a range b values from 0 to about 1000 s/mm^2, or more specifically, flow-sensitive ADC_{low} with lower b values (< 100-200 s/mm^2) and diffusion-sensitive ADC_{high} with higher b values (> 500 s/mm^2) can be quantified. The difference between ADC_{low} and ADC_{high} can be defined as $ADC_{perfusion}$ to assess the perfusion fraction roughly[59,110] (Figure 3). Taking advantage of simplified calculation, mono-exponential analysis neglects the non-linearity of signal decay. To characterize the decay curve more adequately, bi- or multi-exponential models, as well as their alternative method, stretched model, are also explored in order to derive the perfusion fraction (f) and true diffusion coefficient (D). Despite the wider range of b values, longer acquisition time and requirement for higher SNR, the advantage of these more complicated models over mono-exponential methods still needs to be fully elucidated[8,108,111]. For any analytic method, the noise should be reduced whenever possible to ensure accurate fitting of ADC.

Visual interpretation: DW images can be evaluated on source DWI or quantitative ADC maps. DWI with b = 50 s/mm^2 is often called black blood imaging, due to its nullification of blood signals to render vessels black. Black blood DWI has a better detection rate for small tumor lesions than T2WI has[112], and has been recommended as

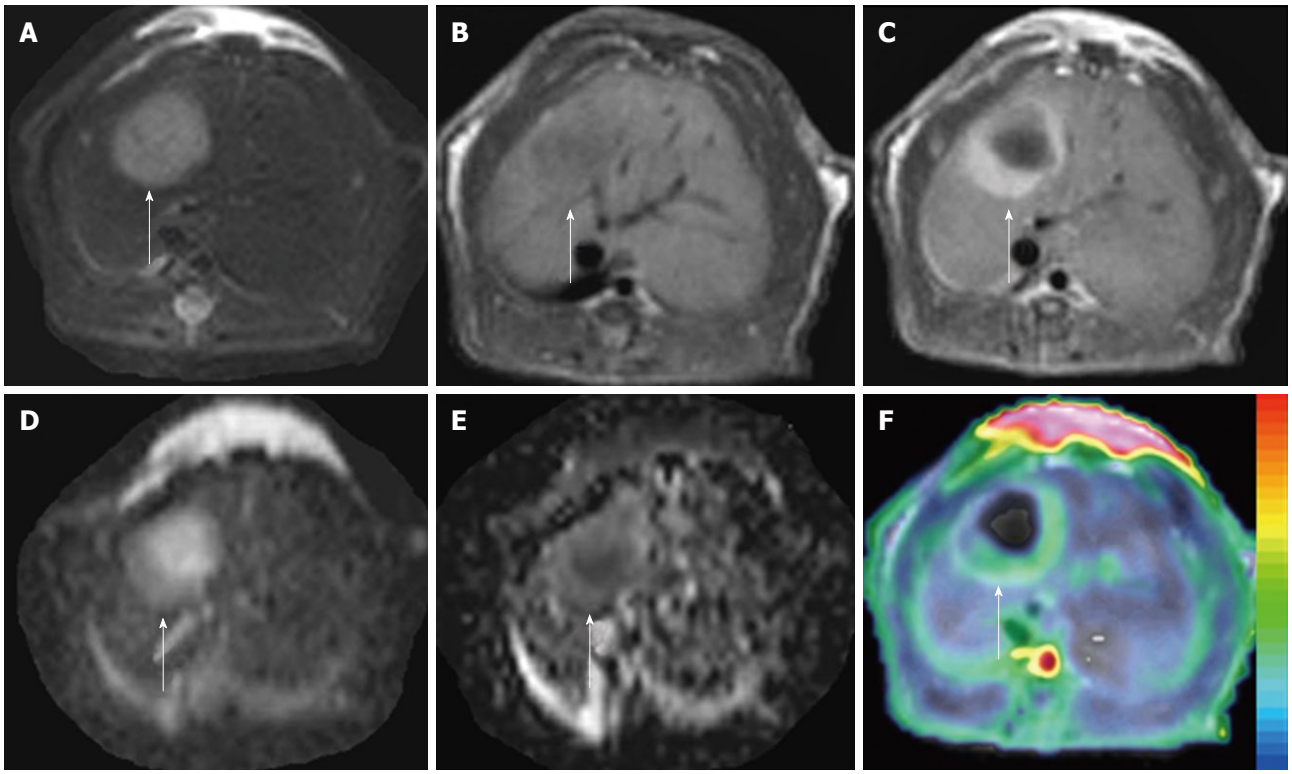

Figure 3 $ADC_{perfusion}$ and initial area under the gadolinium curve in an implanted tumor in rat liver. At 48 h after iv treatment with CA4P at 10 mg/kg, obvious tumor recurrence with partial recovery of blood supply was demonstrated. The tumor (arrows) appeared hyperintense on T2WI (A) and hypointense on T1WI (B); On CE-T1WI, the tumor relapsed at the periphery, shown as ring enhancement of viable tumor cells (C); ADC_{10b} (derived from 10 b values from 0 to 1000 s/mm^2) revealed the hyperintense necrotic center and isointense viable tumor rim (D); On $ADC_{perfusion}$ (ADC_{low}-ADC_{high}) maps, the relative hyperintensity at the periphery suggested the partial recovery of perfusion, compared to the hypointensity in the necrotic center with perfusion deficit (E); $ADC_{perfusion}$ matched well with CE-T1WI-overlyaed initial area under the gadolinium curve (IAUGC) map (F).

an alternative to T2WI with conspicuity of small lesion on 3.0 T scanners[113]. The combination of DWI with T2WI and CE-T1WI has been suggested to improve the diagnostic accuracy of small tumor lesions[94]. However, due to T2 shine-through, hyperintensity on high b value (800-1000 s/mm^2) images does not always indicate increased cellularity, e.g. fluid shows hyperintense on both DWI and ADC maps. For this reason, ADC maps are preferable to DWI, and DWI should be always interpreted concurrently with the ADC map and all other available morphological images to prevent misinterpretation[104].

For the display of DWI or ADC maps, the inverted gray-scale (PET-like) for the suppression of background signal is used for whole-body DWI of high contrast from high b values, to detect multiple metastatic lesions[114]. With the co-registration between DWI or ADC maps with a color scale and structural T1WI or T2WI, fusion imaging can be obtained to integrate functional and anatomic information[8,94].

Quantitative interpretation: For the quantification of ADC, the most frequently used method is to draw a free-hand region of interest (ROI) or volume of interest (VOI) over the whole tumor, and mean or median values of all pixels/voxels within the ROI/VOI are obtained. Such manual delineation is easy but fails to characterize tumor heterogeneity. Histogram-based analysis can reflect the frequency of pixels with different diffusion, and the pixels can be divided into subgroups according to their ADC values. Therefore, it may better reflect how many pixels undergo change in ADC after treatment[8,115]. It has been demonstrated that ADC histogram analysis may be a superior and quicker biomarker of tumor response to bevacizumab than tumor volume[116]. With the spatially varying change in ADC after treatment, an ideal approach is to analyze the pixels present both before and after treatment with spatial tags to detect any change in ADC pixel by pixel. By using a threshold diffusion map, the pixels can be categorized into decrease, increase or no change after treatment. The segmented tumor can be overlaid on structural images to demonstrate clearly the heterogeneous response of a tumor to treatment depending on different locations within the tumor[117]. However, the pixel-wise registration is more susceptible to motion, and its applications in the body is more difficult than in the brain[8].

Evolution of ADC changes: In tumors, the mobility of water molecules is restricted due to cellular membranes or interaction with structural proteins. The high tumor cellularity results in lower diffusivity and thus lower measured ADC in most tumors. However, the restriction on diffusion is multifactorial and also influenced by the unique intracellular water diffusion and microscopic tissue/tumor organizational characteristics. Consequently, the ADC of

untreated tumors can occasionally be higher than that of native tissue[8,110], and it is vital to monitor intrasubject dynamic changes in ADC pre- and post-treatment.

Although the mechanism has not been fully explored, there is a temporary decrease in tumor ADC after VDA treatment. The probable reason may lie in abrupt decline in blood flow, subsequent cytotoxic edema due to the acute hypoxia, and resultant increased tortuosity of water molecules in EES[7,104]. Some preclinical studies have shown a transient decrease in ADC at 1 h after CA4P treatment[107,57]. The duration of decreased ADC was different in these two studies with the same tumor cell line but in different transplantation locations: ADC rebounded to pretreatment values in the intrahepatic tumor at 6 h[57]; however, ADC decreased gradually from 1 h until 6 h in the subcutaneous tumor[107]. The difference in doses of CA4P and tumor locations may have accounted for the phase discrepancy in ADC drop. On the other hand, the reduction in blood flow also contributed to the decrease in ADC[8,110], which was confirmed by the fact that ADC_{low} decreased more significantly than ADC_{high}[56,107].

After the transient drop, ADC rebounds due to the collapsed cell membranes and decreased cellularity, and thus increased mobility of water molecules in EES throughout the progressing necrosis formation, during which the ADC value may reach the pretreatment baseline, and thus shows no significant difference from the baseline at some time points[74]; so-called pseudonormalization of ADC[118]. The onset and duration of pseudonormalization vary depending largely on tumor model and treatment strategy. If MRI falls within the window of pseudonormalization, there can be no significant change in ADC value, which, however, does not necessarily mean that ADC has not dynamically changed.

As necrosis develops, tumor cell volume is reduced with increased EES. The displacement of water molecules is less hampered, which increases ADC. The increase in ADC after VDA treatment has been shown in preclinical and clinical studies[53,57,68,119,120]. The peripheral sparing of tumor after VDA treatment has lower ADC, and can be distinguished from central necrosis of high ADC[8,110] (Figures 2 and 3). After single doses of VDA, the residual tumor unavoidably gives rise to recurrence, which in turn, leads to decreased overall ADC[59].

Derived from the different b values applied in DWI, ADC_{high} mainly reflects the true diffusion and is more accurate for the characterization of VDA-induced necrosis; ADC_{low}, on the other hand, indicates the different weightings by several factors such as diffusion, microcirculation and structural barriers, which deteriorate its measurement reproducibility for individual or intergroup comparisons[119]; and $ADC_{perfusion}$ is most correlated with blood supply and can thus be used to approximate tumor blood perfusion as an alternative when venous access is limited[56,59] (Figure 3).

DCE-MRI

DCE-MRI enables quantitative characterization of microcirculation in terms of blood flow, blood volume and/or capillary permeability, as well as pathophysiological insight into the mechanism of VDA action in tumors. Therefore DCE-MRI has been applied as a promising imaging biomarker for the assessment of VDA effects[121,122].

Basic principles: DCE-MRI involves serial acquisition of sequential images before, during and after injection of a contrast agent to cover the volume of the tumor. By tracking the pharmacokinetics of injected contrast agent, DCE-MRI is capable of the non-invasive quantification of microvascular structure and function. In VDA studies, two kinds of contrast agents are often used: low molecular weight agents (< 1000 Da, e.g. gadolinium diethylenetriaminepentaacetic acid or Gd-DTPA) that rapidly traverse from capillary into the EES, but not into tumor cells; and large molecular agents (> 20 kDa) with low capillary permeability for prolonged intravascular retention, so-called blood pool agents[123]. DCE-MRI sequences can be designed to be T1-weighted or T2*-weighted, which exploit different physiological properties to derive different kinetic variables. T1-weighted DCE-MRI is sensitive to the presence of contrast agent in the EES and reflects microvascular blood flow, permeability and extracellular leakage space, whereas T2*-weighted DCE-MRI, or more specifically, dynamic susceptibility contrast (DSC) MRI, is sensitive to the vascular phase of contrast agent delivery and reflects blood flow and volume[124].

Upon bolus injection, the contrast agent enters arterioles and passes through the capillary network, known as the first pass of the contrast agent. Its paramagnetic properties render a decrease in both the T1 and T2* (or T2) relaxation times of water molecules. On T2*-weighted DEC-MRI, the transient drop of SI of nearby tissue is due to the presence of contrast agent within the capillary compartment. Therefore, such a sequence performs better in brain with intact blood brain barrier (BBB) or when combined with blood pool contrast agents, since the tracer largely remains intravascular[125]. Measurement of the T2* effect during the rapid decrease and subsequent recovery in SI necessitates rapid sampling acquisition to ensure high temporal resolution. T2*-weighted DEC-MRI is mostly applied in brain tumors due to the presence of the BBB[124,126]. In extracranial tumors, the contrast agent readily extravasates from the intravascular space into the EES at a rate determined by several physiological factors including tissue blood flow, permeability of the capillaries and surface area. On T1-weighted DCE-MRI, contrast agent in EES shortens the T_1 relaxation time of nearby water hydrogen nuclei and causes increased SI. Therefore, T1-weighted DEC-MRI is widely applied in the extracranial tumors[127].

Quantification of DCE-MRI: For the quantification of DCE-MRI, we need to convert SI into the concentration of contrast agent at each time point during the acquisition. This is accomplished by measuring the T1 map on T1-weighted DCE-MRI, while it is more complicated in

T2*-weighted DCE-MRI. It is usually necessary to derive arterial input function (AIF) by measuring the SI in arteries near the locations of tumor, and AIF is useful for the compensation of the influence of injection speed of contrast agent and cardiac output[128].

T2*-weighted DCE-MRI: The quantification of T2*-weighted DCE-MRI can be semi-quantitative or quantitative. The former method does not employ complicated kinetic modeling or AIF, and derived summary parameters from contrast agent concentration time curve (or SI time curve) include area under the peak (AUP), and time to peak (TTP). Such analysis is straightforward, while it does not provide pathophysiological information of perfusion related to vascular shutdown[129], and may also be complicated with the leakage of contrast agent into the EES, which is likely in tumors with high permeability[130].

For quantitative analysis of T2*-weighted DCE-MRI, the most robust biomarker is relative blood volume (rBV) from the first-pass technique, calculated as the integral area under the concentration-time curve, with the interpretation of AIF and kinetic models[131]. Relative blood flow can also be quantified, and mean transit time (MTT) is obtained according to the central volume theorem BF = BV/MTT. However, extracranial tumors are usually hyperpermeable, and the compartmentalization of contrast agent is usually lost. Thus quantification of these parameters are less reliable due to the leakage of contrast agent into the EES and subsequent T1 effect on T2*-weighted sequence. The possible solutions include the correction with gamma-variate function by using more complicated kinetic models, preloaded dose of contrast agent to eliminate the effect of its leakage into the EES or its recirculation, and dual or multiecho imaging sequences[130,132-135].

T1-weighted DCE-MRI: T1-weighed DCE-MRI exploits the distribution of contrast agent in the EES, which increases the T1 relaxation rate (1/T1) of nearby hydrogen nuclei. The concentration of gadolinium ions is known to be directly proportional to the change in 1/T1, and the latter is related to changes in SI on T1WI. With a low gadolinium dose, we can assume that there is a linear relation between the amount of contrast agent in the tissue and the resultant difference in relaxation time[136]. Semi-quantitative and quantitative analyses of T1-weighted DCE-MRI are possible.

For semi-quantitative analysis, the model-free method utilizes the enhancement curve in terms of curve shape, time from injection to arrival of contrast agent, gradient of upslope or wash out phase and maximal intensity[124]. The most frequently used parameter is initial area under the gadolinium curve (IAUGC) (Figure 3), as well as maximal initial slope of curve, TTP, and the slope of washout[56,127]. The simplicity of this method with computer routine enables its easy accessibility to many investigators, and it has been shown to be successful to monitor the responses to VDA[59,137]. However, these semi-quantitative measures fail to show any direct correlation with underlying physiological measures of tumor perfusion, permeability or leakage space, and only provide a mixed complex that hampers the interpatient or interscanner comparison[122,138].

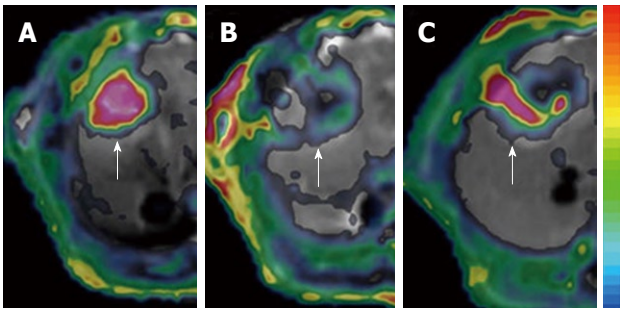

Figure 4 Dynamic changes in K^{trans}. The tumor (arrows) in rat liver showed an abundant blood supply with high K^{trans} before treatment (A); At 6 h after CA4P treatment, vascular shutdown was indicated with low K^{trans} in the center, surrounded by tumor residue at the periphery, with moderate K^{trans} (B); At 48 h after treatment, the tumor relapsed upon the residue at the periphery with rebounding K^{trans} (C).

Quantitative analysis of T1-weighed DCE-MRI involves a pharmacokinetic model to characterize the underlying physiological process of the contrast agent in tissues, including its administration, first pass, transendothelial process, distribution in EES, and wash out[124,139]. On the basis of some simplifying assumptions, biological tissues can be regarded as several compartments, e.g. two-compartment model with blood plasma and EES, within which contrast agent is instantaneously mixed and uniformly distributed[127]. The Tofts model is one of the frequently used pharmacokinetic models to fit concentration-time serial data in order to derive physiological parameters[140,141]. The robust parameters include K^{trans} (volume transfer constant of the contrast agent, unit/min), K_{ep} (rate constant of wash out of contrast agent refluxing from EES into blood, unit/min) and V_e (the extravascular extracellular volume fraction, unit %).

Although quantification of K^{trans} is often overestimated due to the innate assumptions in all kinetic models[142], and dedicated software has to be involved in the analysis, quantitative analysis of T1-weighted DCE-MRI highlights the underlying mechanism of VDA action in terms of the permeability change and subsequent perfusion collapse after VDAs, and it facilitates the direct comparison of these physiological parameters for intra- and inter-subject studies (Figure 4). Thus, the imaging biomarkers from DCE-MRI are most correlative to the VDA effects.

Interpretation of DCE-MRI: In general, successful VDA treatment causes the immediate vascular shutdown of tumors, shown as a rapid drop in semi-quantitative and quantitative DCE-MRI parameters within minutes or hours, and neoplastic recurrence is reflected as recovery in such measures to baseline level, which depends on the dose of VDAs and tumor models[7,26,39,53,54,73,143] (Figure 4).

K^{trans} reflects a composite of both blood flow and vascular permeability-area product, and therefore, its interpretation depends on the rate-limiting step between

perfusion in vessels and diffusion into the EES. In untreated tumors, the vascular permeability-area product is often high, and the tissue is described as flow-limited, so that K^{trans} approximates blood flow[140]; after the treatment with VDAs, the permeability transiently increases and then the blood flow drops abruptly, which decreases K^{trans}. However, in this mixed situation, the blood flow and permeability cannot be decoupled and it is difficult to identify the dominating factor between the perfusion and permeability-area product[56,124,140] (Figure 4).

For example, in a rat subcutaneous tumor model, tumor perfusion decreased by 57% with ABT-751 treatment after 1 h, but recovered to near pretreatment levels within 6 h[59]. In a rat liver tumor model with ZD6126 treatment, K^{trans} dropped to its lowest at 24 h and partially recovered at 48 h[56], while for the same tumor cell line but in subcutaneous model with CA4P, K^{trans} decreased to its lowest level at 6 h and recovered at 9 d[59]. Values of DCE-MRI parameters are derived from an ROI covering the whole tumor in most studies, which however, ignores the tumor heterogeneity due to the persistence of the viable rim after VDA treatment. Therefore, inclusion of non-enhancing pixels in the center artificially underestimates the mean and/or median parameter values[144]. Some authors have defined the tumor center and periphery and have analyzed the DCE-MRI parameters respectively, and have successfully shown the different responses in necrotic center and viable rim, which have helped to elucidate tumor pathophysiology and drug action of VDAs[46]. However, the definition of core and rim is debatable[145] and manual delineation of tumor center and periphery suffers from relatively poor spatial resolution on DCE-MRI, even with cross reference to other structural images of higher spatial resolution such as that derived from CE-T1WI.

Alternatively, pixel-based analysis of DCE-MRI quantifies the value of each pixel within a tumor, and distribution histogram and mean and/or median values can be derived, which is especially helpful in the dynamic follow-up of VDA treatment[146,147]. Nonetheless, this pixel-based method suffers more from motion artifacts in extracranial tumors, than whole-tumor-based analysis, and the technique remains challenging for physiological motion, such as cardiac and respiratory movements[148].

VALIDATION OF MRI FINDINGS

The tumor response to VDA treatment has been widely validated using a number of methods. As an established index for determining VDA treatment efficacy, treatment-induced necrosis, as well as cytotoxic edema, has been confirmed with postmortem histopathology[57,107]. Necrosis has been an established end point of drug response with histopathological proofs in preclinical VDA studies, and the extent of necrosis is consistent with the DCE-MRI parameters. Considering uneasily accessible histopathology in patients, DCE-MRI is regarded as a promising biomarker to demonstrate the VDA-induced necrosis in patients[149].

Unfortunately, the validation of VDA-induced vascular collapse with resultant stoppage of tumor blood supply is still technically challenging due to a lack of more robust methods. One frequently adopted method is microvascular density (MVD) determination with immunohistochemical staining by using vascular markers such as CD31, CD34 or CD105[150]. Some studies with antiangiogenic treatment have shown a correlation between DCE-MRI parameters and immunohistochemical findings, whereas others have not[133]. There is a paucity of such correlation data in VDA studies. Gaya *et al*[151] have shown no strong relationship between changes in DCE-MRI kinetic variables following CA4P and the immunohistochemical angiogenic profile. There is always a discrepancy between histological MVD and functional vascular density: not all tumor vessels are perfused at a given time[124], and it is not surprising that MVD fails to characterize the functional properties including vessel permeability, which contribute to DCE-MRI parameters. On the other hand, blood vessels are often distended early after VDA treatment, with severe comprise of blood flow, which can be false-negative on MVD measurement[152]. Accordingly, its value as an indicator of the efficacy of VDA therapies is limited[153]. In other words, the absence of decreased MVD does not necessarily indicate ineffective VDA treatment[150]. Alternatively, Hoechst 33342 is a dye that stains the nuclei of ECs lining blood vessels that are perfused at the time of injection, and therefore, may provide a better histological measurement of functional vasculature *via* fluorescence microscopy after VDA treatment[149,153-155].

In a rat tumor model treated with CA4P, Maxwell *et al*[156] have compared K^{trans} with tumor blood flow measured by the uptake of radiolabeled iodoantipyrine (IAP). They have shown that dynamic changes in K^{trans} and AUC, and tumor blood flow from IAP uptake after treatment are highly correlated, although with the changes in K^{trans} and AUC being smaller than those in blood flow by IAP. However, it is still uncertain to what extent K^{trans} can mirror the blood flow changes, especially in the condition limited by permeability-surface area product, which may be the case in extracranial tumors after VDA treatment[156,157]. In VDA studies, the correlation still needs to be explored with other robust techniques such as H215O-PET[158] and microbubble ultrasound[159].

FUTURE PERSPECTIVES

Multiparametric MRI biomarkers enable non-invasive characterization of tumor response to VDA, while the variety of biomarkers also leads to the challenges in terms of robust protocol for standardization of imaging acquisition and analysis on intrasubject or intersubject basis. Therefore, it is imperative to develop a standardized protocol to facilitate the comparative evaluation of VDA treatment effects in multicenter studies.

Due to practical limitations, advanced MRI methods of imaging acquisition and analysis for DWI and DCE-MRI are only accessible in research centers with expertise.

However, this should not be a hurdle to perform examinations. Therefore, to circumvent technical limitations, a hierarchical protocol with compromises can be expected, in which the protocols from the most ideal conditions to some practical alternatives are given, according to their relevance to the insight of pathophysiological mechanisms of VDA action[56].

Heterogeneity is involved throughout VDA treatment: tumors can be responders or non-responders to VDAs; the response degree can vary; and most importantly, tumor residue unavoidably remains at the periphery due to the incomplete tumoricidal effect of VDAs. The most adopted whole-tumor-based quantitative analysis neglects the spatial heterogeneity with central necrosis and peripheral sparing, which, however, may affect therapeutic evaluation and prognostic prediction for the adjustment of individual therapy strategy[144]. Other alternatives such as co-registration between pre- and post-treatment images facilitate the pixel-based demonstration of treatment response, although they are still problematic for application in areas with significant movement, such as the abdomen[117].

It is only by combining multiparametric imaging biomarkers that we may begin to understand how VDAs affect tissue environment and tumor cells. To date, DCE-MRI and DWI, as well as ^{18}F fluorodeoxyglucose PET are the most advanced biomarkers, from which we can gain insights into vascular function, programmed cell death or necrosis, and glucose metabolism. However, procedural rigor of these multiparametric imaging biomarkers has to be established before they can take up an essential position in clinical decision making[56,160].

CONCLUSION

Considering the requirements of prompt therapeutic justification and adjustment for oncological patients with VDA treatment, there are urgent demands for establishing comprehensive imaging protocol for "go or no-go" clinical decisions. Investigations in preclinical animal models can provide the insights into the mechanism of VDA action; realized by applying multiparametric imaging biomarkers with validation at microscopic levels. Therefore, it is possible that combination of these quantitative imaging biomarkers, especially DWI and DCE-MRI, can play an imperative role in clinical treatment regimens that involve VDAs. Standardization of imaging acquisition and analysis with advanced hardware and software needs to be developed to improve the accuracy and comparability of VDA studies in multicenter studies.

REFERENCES

1 **Brown JM**, Giaccia AJ. The unique physiology of solid tumors: opportunities (and problems) for cancer therapy. *Cancer Res* 1998; **58**: 1408-1416
2 **Fukumura D**, Jain RK. Tumor microvasculature and microenvironment: targets for anti-angiogenesis and normalization. *Microvasc Res* 2007; **74**: 72-84
3 **Vaupel P**, Kallinowski F, Okunieff P. Blood flow, oxygen and nutrient supply, and metabolic microenvironment of human tumors: a review. *Cancer Res* 1989; **49**: 6449-6465
4 **Fidler IJ**. Angiogenic heterogeneity: regulation of neoplastic angiogenesis by the organ microenvironment. *J Natl Cancer Inst* 2001; **93**: 1040-1041
5 **Lippert JW 3rd**. Vascular disrupting agents. *Bioorg Med Chem* 2007; **15**: 605-615
6 **Heath VL**, Bicknell R. Anticancer strategies involving the vasculature. *Nat Rev Clin Oncol* 2009; **6**: 395-404
7 **Kanthou C**, Tozer GM. Microtubule depolymerizing vascular disrupting agents: novel therapeutic agents for oncology and other pathologies. *Int J Exp Pathol* 2009; **90**: 284-294
8 **Padhani AR**, Liu G, Koh DM, Chenevert TL, Thoeny HC, Takahara T, Dzik-Jurasz A, Ross BD, Van Cauteren M, Collins D, Hammoud DA, Rustin GJ, Taouli B, Choyke PL. Diffusion-weighted magnetic resonance imaging as a cancer biomarker: consensus and recommendations. *Neoplasia* 2009; **11**: 102-125
9 **Smith JJ**, Sorensen AG, Thrall JH. Biomarkers in imaging: realizing radiology's future. *Radiology* 2003; **227**: 633-638
10 **Murphy PS**, McCarthy TJ, Dzik-Jurasz AS. The role of clinical imaging in oncological drug development. *Br J Radiol* 2008; **81**: 685-692
11 **Jain RK**. Barriers to drug delivery in solid tumors. *Sci Am* 1994; **271**: 58-65
12 **Gimbrone MA Jr**, Cotran RS, Leapman SB, Folkman J. Tumor growth and neovascularization: an experimental model using the rabbit cornea. *J Natl Cancer Inst* 1974; **52**: 413-427
13 **Thomlinson RH**, Gray LH. The histological structure of some human lung cancers and the possible implications for radiotherapy. *Br J Cancer* 1955; **9**: 539-549
14 **Folkman J**. Role of angiogenesis in tumor growth and metastasis. *Semin Oncol* 2002; **29**: 15-18
15 **Dvorak HF**, Nagy JA, Dvorak JT, Dvorak AM. Identification and characterization of the blood vessels of solid tumors that are leaky to circulating macromolecules. *Am J Pathol* 1988; **133**: 95-109
16 **Hashizume H**, Baluk P, Morikawa S, McLean JW, Thurston G, Roberge S, Jain RK, McDonald DM. Openings between defective endothelial cells explain tumor vessel leakiness. *Am J Pathol* 2000; **156**: 1363-1380
17 **Paku S**, Paweletz N. First steps of tumor-related angiogenesis. *Lab Invest* 1991; **65**: 334-346
18 **Baluk P**, Morikawa S, Haskell A, Mancuso M, McDonald DM. Abnormalities of basement membrane on blood vessels and endothelial sprouts in tumors. *Am J Pathol* 2003; **163**: 1801-1815
19 **Leu AJ**, Berk DA, Lymboussaki A, Alitalo K, Jain RK. Absence of functional lymphatics within a murine sarcoma: a molecular and functional evaluation. *Cancer Res* 2000; **60**: 4324-4327
20 **Padera TP**, Stoll BR, Tooredman JB, Capen D, di Tomaso E, Jain RK. Pathology: cancer cells compress intratumour vessels. *Nature* 2004; **427**: 695
21 **Sevick EM**, Jain RK. Geometric resistance to blood flow in solid tumors perfused ex vivo: effects of tumor size and perfusion pressure. *Cancer Res* 1989; **49**: 3506-3512
22 **Bogatcheva NV**, Verin AD. Reprint of "The role of cytoskeleton in the regulation of vascular endothelial barrier function" [Microvascular Research 76 (2008) 202-207]. *Microvasc Res* 2009; **77**: 64-69
23 **Pasquier E**, Kavallaris M. Microtubules: a dynamic target in cancer therapy. *IUBMB Life* 2008; **60**: 165-170
24 **Lee TY**, Gotlieb AI. Microfilaments and microtubules maintain endothelial integrity. *Microsc Res Tech* 2003; **60**: 115-127
25 **Thorpe PE**. Vascular targeting agents as cancer therapeutics. *Clin Cancer Res* 2004; **10**: 415-427
26 **Siemann DW**, Chaplin DJ, Walicke PA. A review and update of the current status of the vasculature-disabling agent combretastatin-A4 phosphate (CA4P). *Expert Opin Investig Drugs*

2009; **18**: 189-197
27 **Schwartz EL**. Antivascular actions of microtubule-binding drugs. *Clin Cancer Res* 2009; **15**: 2594-2601
28 **Lee RM**, Gewirtz DA. Colchicine site inhibitors of microtubule integrity as vascular disrupting agents. *Drug Dev Res* 2008; **69**: 352-358
29 **Jordan MA**, Wilson L. Microtubules as a target for anticancer drugs. *Nat Rev Cancer* 2004; **4**: 253-265
30 **Anderson HL**, Yap JT, Miller MP, Robbins A, Jones T, Price PM. Assessment of pharmacodynamic vascular response in a phase I trial of combretastatin A4 phosphate. *J Clin Oncol* 2003; **21**: 2823-2830
31 **Wittmann T**, Waterman-Storer CM. Cell motility: can Rho GTPases and microtubules point the way? *J Cell Sci* 2001; **114**: 3795-3803
32 **Boureux A**, Vignal E, Faure S, Fort P. Evolution of the Rho family of ras-like GTPases in eukaryotes. *Mol Biol Evol* 2007; **24**: 203-216
33 **Bustelo XR**, Sauzeau V, Berenjeno IM. GTP-binding proteins of the Rho/Rac family: regulation, effectors and functions in vivo. *Bioessays* 2007; **29**: 356-370
34 **Waterman-Storer CM**, Salmon E. Positive feedback interactions between microtubule and actin dynamics during cell motility. *Curr Opin Cell Biol* 1999; **11**: 61-67
35 **Birukova AA**, Adyshev D, Gorshkov B, Bokoch GM, Birukov KG, Verin AD. GEF-H1 is involved in agonist-induced human pulmonary endothelial barrier dysfunction. *Am J Physiol Lung Cell Mol Physiol* 2006; **290**: L540-L548
36 **Kanthou C**, Tozer GM. The tumor vascular targeting agent combretastatin A-4-phosphate induces reorganization of the actin cytoskeleton and early membrane blebbing in human endothelial cells. *Blood* 2002; **99**: 2060-2069
37 **Houle F**, Huot J. Dysregulation of the endothelial cellular response to oxidative stress in cancer. *Mol Carcinog* 2006; **45**: 362-367
38 **Tozer GM**, Prise VE, Wilson J, Cemazar M, Shan S, Dewhirst MW, Barber PR, Vojnovic B, Chaplin DJ. Mechanisms associated with tumor vascular shut-down induced by combretastatin A-4 phosphate: intravital microscopy and measurement of vascular permeability. *Cancer Res* 2001; **61**: 6413-6422
39 **Luo Y**, Hradil VP, Frost DJ, Rosenberg SH, Gordon GB, Morgan SJ, Gagne GD, Cox BF, Tahir SK, Fox GB. ABT-751, a novel tubulin-binding agent, decreases tumor perfusion and disrupts tumor vasculature. *Anticancer Drugs* 2009; **20**: 483-492
40 **Tozer GM**, Kanthou C, Baguley BC. Disrupting tumour blood vessels. *Nat Rev Cancer* 2005; **5**: 423-435
41 **Tozer GM**, Kanthou C, Parkins CS, Hill SA. The biology of the combretastatins as tumour vascular targeting agents. *Int J Exp Pathol* 2002; **83**: 21-38
42 **Yeung SC**, She M, Yang H, Pan J, Sun L, Chaplin D. Combination chemotherapy including combretastatin A4 phosphate and paclitaxel is effective against anaplastic thyroid cancer in a nude mouse xenograft model. *J Clin Endocrinol Metab* 2007; **92**: 2902-2909
43 **Ishizaki T**, Uehata M, Tamechika I, Keel J, Nonomura K, Maekawa M, Narumiya S. Pharmacological properties of Y-27632, a specific inhibitor of rho-associated kinases. *Mol Pharmacol* 2000; **57**: 976-983
44 **Vincent L**, Kermani P, Young LM, Cheng J, Zhang F, Shido K, Lam G, Bompais-Vincent H, Zhu Z, Hicklin DJ, Bohlen P, Chaplin DJ, May C, Rafii S. Combretastatin A4 phosphate induces rapid regression of tumor neovessels and growth through interference with vascular endothelial-cadherin signaling. *J Clin Invest* 2005; **115**: 2992-3006
45 **Burns CJ**, Fantino E, Phillips ID, Su S, Harte MF, Bukczynska PE, Frazzetto M, Joffe M, Kruszelnicki I, Wang B, Wang Y, Wilson N, Dilley RJ, Wan SS, Charman SA, Shackleford DM, Fida R, Malcontenti-Wilson C, Wilks AF. CYT997: a novel orally active tubulin polymerization inhibitor with potent cytotoxic and vascular disrupting activity in vitro and in vivo. *Mol Cancer Ther* 2009; **8**: 3036-3045
46 **Galbraith SM**, Maxwell RJ, Lodge MA, Tozer GM, Wilson J, Taylor NJ, Stirling JJ, Sena L, Padhani AR, Rustin GJ. Combretastatin A4 phosphate has tumor antivascular activity in rat and man as demonstrated by dynamic magnetic resonance imaging. *J Clin Oncol* 2003; **21**: 2831-2842
47 **Prise VE**, Honess DJ, Stratford MR, Wilson J, Tozer GM. The vascular response of tumor and normal tissues in the rat to the vascular targeting agent, combretastatin A-4-phosphate, at clinically relevant doses. *Int J Oncol* 2002; **21**: 717-726
48 **Tozer GM**, Prise VE, Lewis G, Xie S, Wilson I, Hill SA. Nitric oxide synthase inhibition enhances the tumor vascular-damaging effects of combretastatin a-4 3-o-phosphate at clinically relevant doses. *Clin Cancer Res* 2009; **15**: 3781-3790
49 **Dark GG**, Hill SA, Prise VE, Tozer GM, Pettit GR, Chaplin DJ. Combretastatin A-4, an agent that displays potent and selective toxicity toward tumor vasculature. *Cancer Res* 1997; **57**: 1829-1834
50 **Rustin GJ**, Galbraith SM, Anderson H, Stratford M, Folkes LK, Sena L, Gumbrell L, Price PM. Phase I clinical trial of weekly combretastatin A4 phosphate: clinical and pharmacokinetic results. *J Clin Oncol* 2003; **21**: 2815-2822
51 **Bradley DP**, Tessier JJ, Ashton SE, Waterton JC, Wilson Z, Worthington PL, Ryan AJ. Correlation of MRI biomarkers with tumor necrosis in Hras5 tumor xenograft in athymic rats. *Neoplasia* 2007; **9**: 382-391
52 **Davis PD**, Dougherty GJ, Blakey DC, Galbraith SM, Tozer GM, Holder AL, Naylor MA, Nolan J, Stratford MR, Chaplin DJ, Hill SA. ZD6126: a novel vascular-targeting agent that causes selective destruction of tumor vasculature. *Cancer Res* 2002; **62**: 7247-7253
53 **Chen G**, Horsman MR, Pedersen M, Pang Q, Stødkilde-Jørgensen H. The effect of combretastatin A4 disodium phosphate and 5,6-dimethylxanthenone-4-acetic acid on water diffusion and blood perfusion in tumours. *Acta Oncol* 2008; **47**: 1071-1076
54 **Delmonte A**, Sessa C. AVE8062: a new combretastatin derivative vascular disrupting agent. *Expert Opin Investig Drugs* 2009; **18**: 1541-1548
55 **Sheng Y**, Hua J, Pinney KG, Garner CM, Kane RR, Prezioso JA, Chaplin DJ, Edvardsen K. Combretastatin family member OXI4503 induces tumor vascular collapse through the induction of endothelial apoptosis. *Int J Cancer* 2004; **111**: 604-610
56 **Wang H**, Li J, Chen F, De Keyzer F, Yu J, Feng Y, Nuyts J, Marchal G, Ni Y. Morphological, functional and metabolic imaging biomarkers: assessment of vascular-disrupting effect on rodent liver tumours. *Eur Radiol* 2010; **20**: 2013-2026
57 **Wang H**, Sun X, Chen F, De Keyzer F, Yu J, Landuyt W, Vandecaveye V, Peeters R, Bosmans H, Hermans R, Marchal G, Ni Y. Treatment of rodent liver tumor with combretastatin a4 phosphate: noninvasive therapeutic evaluation using multiparametric magnetic resonance imaging in correlation with microangiography and histology. *Invest Radiol* 2009; **44**: 44-53
58 **Dachs GU**, Steele AJ, Coralli C, Kanthou C, Brooks AC, Gunningham SP, Currie MJ, Watson AI, Robinson BA, Tozer GM. Anti-vascular agent Combretastatin A-4-P modulates hypoxia inducible factor-1 and gene expression. *BMC Cancer* 2006; **6**: 280
59 **Thoeny HC**, De Keyzer F, Vandecaveye V, Chen F, Sun X, Bosmans H, Hermans R, Verbeken EK, Boesch C, Marchal G, Landuyt W, Ni Y. Effect of vascular targeting agent in rat tumor model: dynamic contrast-enhanced versus diffusion-weighted MR imaging. *Radiology* 2005; **237**: 492-499
60 **Siim BG**, Laux WT, Rutland MD, Palmer BN, Wilson WR. Scintigraphic imaging of the hypoxia marker (99m)technetium-labeled 2,2'-(1,4-diaminobutane)bis(2-methyl-3-butanone) dioxime (99mTc-labeled HL-91; prognox): noninvasive detection of tumor response to the antivascular agent 5,6-dimethylxanthenone-4-acetic acid. *Cancer Res* 2000;

60: 4582-4588
61 **Siemann DW**, Shi W. Dual targeting of tumor vasculature: combining Avastin and vascular disrupting agents (CA4P or OXi4503). *Anticancer Res* 2008; **28**: 2027-2031
62 **Seshadri M**, Bellnier DA, Cheney RT. Assessment of the early effects of 5,6-dimethylxanthenone-4-acetic acid using macromolecular contrast media-enhanced magnetic resonance imaging: ectopic versus orthotopic tumors. *Int J Radiat Oncol Biol Phys* 2008; **72**: 1198-1207
63 **Grosios K**, Holwell SE, McGown AT, Pettit GR, Bibby MC. In vivo and in vitro evaluation of combretastatin A-4 and its sodium phosphate prodrug. *Br J Cancer* 1999; **81**: 1318-1327
64 **Seshadri M**, Toth K. Acute vascular disruption by 5,6-dimethylxanthenone-4-acetic Acid in an orthotopic model of human head and neck cancer. *Transl Oncol* 2009; **2**: 121-127
65 **Kleespies A**, Köhl G, Friedrich M, Ryan AJ, Barge A, Jauch KW, Bruns CJ. Vascular targeting in pancreatic cancer: the novel tubulin-binding agent ZD6126 reveals antitumor activity in primary and metastatic tumor models. *Neoplasia* 2005; **7**: 957-966
66 **Liu JJ**, Ching LM, Goldthorpe M, Sutherland R, Baguley BC, Kirker JA, McKeage MJ. Antitumour action of 5,6-dimethylxanthenone-4-acetic acid in rats bearing chemically induced primary mammary tumours. *Cancer Chemother Pharmacol* 2007; **59**: 661-669
67 **McPhail LD**, Chung YL, Madhu B, Clark S, Griffiths JR, Kelland LR, Robinson SP. Tumor dose response to the vascular disrupting agent, 5,6-dimethylxanthenone-4-acetic acid, using in vivo magnetic resonance spectroscopy. *Clin Cancer Res* 2005; **11**: 3705-3713
68 **Vogel-Claussen J**, Gimi B, Artemov D, Bhujwalla ZM. Diffusion-weighted and macromolecular contrast enhanced MRI of tumor response to antivascular therapy with ZD6126. *Cancer Biol Ther* 2007; **6**: 1469-1475
69 **Thomas CD**, Walczak C, Kaffy J, Pontikis R, Jouanneau J, Volk A. Early effects of combretastatin A4 phosphate assessed by anatomic and carbogen-based functional magnetic resonance imaging on rat bladder tumors implanted in nude mice. *Neoplasia* 2006; **8**: 587-595
70 **Wankhede M**, Dedeugd C, Siemann DW, Sorg BS. In vivo functional differences in microvascular response of 4T1 and Caki-1 tumors after treatment with OXi4503. *Oncol Rep* 2010; **23**: 685-692
71 **Breidahl T**, Nielsen FU, Stødkilde-Jørgensen H, Maxwell RJ, Horsman MR. The effects of the vascular disrupting agents combretastatin A-4 disodium phosphate, 5,6-dimethylxanthenone-4-acetic acid and ZD6126 in a murine tumour: a comparative assessment using MRI and MRS. *Acta Oncol* 2006; **45**: 306-316
72 **Ni Y**, Wang H, Chen F, Li J, DeKeyzer F, Feng Y, Yu J, Bosmans H, Marchal G. Tumor models and specific contrast agents for small animal imaging in oncology. *Methods* 2009; **48**: 125-138
73 **Stevenson JP**, Rosen M, Sun W, Gallagher M, Haller DG, Vaughn D, Giantonio B, Zimmer R, Petros WP, Stratford M, Chaplin D, Young SL, Schnall M, O'Dwyer PJ. Phase I trial of the antivascular agent combretastatin A4 phosphate on a 5-day schedule to patients with cancer: magnetic resonance imaging evidence for altered tumor blood flow. *J Clin Oncol* 2003; **21**: 4428-4438
74 **Beauregard DA**, Thelwall PE, Chaplin DJ, Hill SA, Adams GE, Brindle KM. Magnetic resonance imaging and spectroscopy of combretastatin A4 prodrug-induced disruption of tumour perfusion and energetic status. *Br J Cancer* 1998; **77**: 1761-1767
75 **Madhu B**, Waterton JC, Griffiths JR, Ryan AJ, Robinson SP. The response of RIF-1 fibrosarcomas to the vascular-disrupting agent ZD6126 assessed by in vivo and ex vivo 1H magnetic resonance spectroscopy. *Neoplasia* 2006; **8**: 560-567
76 **Kuhl CK**, Träber F, Schild HH. Whole-body high-field-strength (3.0-T) MR Imaging in Clinical Practice. Part I. Technical considerations and clinical applications. *Radiology* 2008; **246**: 675-696
77 **Willinek WA**, Schild HH. Clinical advantages of 3.0 T MRI over 1.5 T. *Eur J Radiol* 2008; **65**: 2-14
78 **Barth MM**, Smith MP, Pedrosa I, Lenkinski RE, Rofsky NM. Body MR imaging at 3.0 T: understanding the opportunities and challenges. *Radiographics* 2007; **27**: 1445-1462; discussion 1462-1464
79 **Di Costanzo A**, Pollice S, Trojsi F, Giannatempo GM, Popolizio T, Canalis L, Armillotta M, Maggialetti A, Carriero A, Tedeschi G, Scarabino T. Role of perfusion-weighted imaging at 3 Tesla in the assessment of malignancy of cerebral gliomas. *Radiol Med* 2008; **113**: 134-143
80 **Akisik FM**, Sandrasegaran K, Aisen AM, Lin C, Lall C. Abdominal MR imaging at 3.0 T. *Radiographics* 2007; **27**: 1433-1444; discussion 1462-1464
81 **Kuhl CK**, Träber F, Gieseke J, Drahanowsky W, Morakkabati-Spitz N, Willinek W, von Falkenhausen M, Manka C, Schild HH. Whole-body high-field-strength (3.0-T) MR imaging in clinical practice. Part II. Technical considerations and clinical applications. *Radiology* 2008; **247**: 16-35
82 **Chen G**, Jespersen S, Pedersen M, Pang Q, Horsman MR, Stødkilde Jørgensen H. Evaluation of anti-vascular therapy with texture analysis. *Anticancer Res* 2005; **25**: 3399-3405
83 **Therasse P**, Arbuck SG, Eisenhauer EA, Wanders J, Kaplan RS, Rubinstein L, Verweij J, Van Glabbeke M, van Oosterom AT, Christian MC, Gwyther SG. New guidelines to evaluate the response to treatment in solid tumors. European Organization for Research and Treatment of Cancer, National Cancer Institute of the United States, National Cancer Institute of Canada. *J Natl Cancer Inst* 2000; **92**: 205-216
84 **Dempsey MF**, Condon BR, Hadley DM. Measurement of tumor "size" in recurrent malignant glioma: 1D, 2D, or 3D? *AJNR Am J Neuroradiol* 2005; **26**: 770-776
85 **Warren KE**, Patronas N, Aikin AA, Albert PS, Balis FM. Comparison of one-, two-, and three-dimensional measurements of childhood brain tumors. *J Natl Cancer Inst* 2001; **93**: 1401-1405
86 **Koh DM**, Padhani AR. Diffusion-weighted MRI: a new functional clinical technique for tumour imaging. *Br J Radiol* 2006; **79**: 633-635
87 **Lencioni R**, Llovet JM. Modified RECIST (mRECIST) assessment for hepatocellular carcinoma. *Semin Liver Dis* 2010; **30**: 52-60
88 **Bruix J**, Sherman M, Llovet JM, Beaugrand M, Lencioni R, Burroughs AK, Christensen E, Pagliaro L, Colombo M, Rodés J. Clinical management of hepatocellular carcinoma. Conclusions of the Barcelona-2000 EASL conference. European Association for the Study of the Liver. *J Hepatol* 2001; **35**: 421-430
89 **Lang P**, Wendland MF, Saeed M, Gindele A, Rosenau W, Mathur A, Gooding CA, Genant HK. Osteogenic sarcoma: noninvasive in vivo assessment of tumor necrosis with diffusion-weighted MR imaging. *Radiology* 1998; **206**: 227-235
90 **Schima W**, Ba-Ssalamah A, Kurtaran A, Schindl M, Gruenberger T. Post-treatment imaging of liver tumours. *Cancer Imaging* 2007; **7** Spec No A: S28-S36
91 **Ni Y**, Bormans G, Chen F, Verbruggen A, Marchal G. Necrosis avid contrast agents: functional similarity versus structural diversity. *Invest Radiol* 2005; **40**: 526-535
92 **Ni Y**. Metalloporphyrins and Functional Analogues as MRI Contrast Agents. *Curr Med Imaging Rev* 2008; **4**: 96-112
93 **Chenevert TL**, Stegman LD, Taylor JM, Robertson PL, Greenberg HS, Rehemtulla A, Ross BD. Diffusion magnetic resonance imaging: an early surrogate marker of therapeutic efficacy in brain tumors. *J Natl Cancer Inst* 2000; **92**: 2029-2036
94 **Taouli B**, Koh DM. Diffusion-weighted MR imaging of the liver. *Radiology* 2010; **254**: 47-66
95 **Chiu FY**, Jao JC, Chen CY, Liu GC, Jaw TS, Chiou YY, Hsu FO, Hsu JS. Effect of intravenous gadolinium-DTPA on diffu-

sion-weighted magnetic resonance images for evaluation of focal hepatic lesions. *J Comput Assist Tomogr* 2005; **29**: 176-180
96 **Ogura A**, Hayakawa K, Miyati T, Maeda F. The effect of susceptibility of gadolinium contrast media on diffusion-weighted imaging and the apparent diffusion coefficient. *Acad Radiol* 2008; **15**: 867-872
97 **Bellin MF**, Van Der Molen AJ. Extracellular gadolinium-based contrast media: an overview. *Eur J Radiol* 2008; **66**: 160-167
98 **Prince MR**, Zhang HL, Prowda JC, Grossman ME, Silvers DN. Nephrogenic systemic fibrosis and its impact on abdominal imaging. *Radiographics* 2009; **29**: 1565-1574
99 **Bammer R**. Basic principles of diffusion-weighted imaging. *Eur J Radiol* 2003; **45**: 169-184
100 **Le Bihan D**. Molecular diffusion nuclear magnetic resonance imaging. *Magn Reson Q* 1991; **7**: 1-30
101 **Szafer A**, Zhong J, Anderson AW, Gore JC. Diffusion-weighted imaging in tissues: theoretical models. *NMR Biomed* 1995; **8**: 289-296
102 **Chenevert TL**, Brunberg JA, Pipe JG. Anisotropic diffusion in human white matter: demonstration with MR techniques in vivo. *Radiology* 1990; **177**: 401-405
103 **Le Bihan D**, Breton E, Lallemand D, Aubin ML, Vignaud J, Laval-Jeantet M. Separation of diffusion and perfusion in intravoxel incoherent motion MR imaging. *Radiology* 1988; **168**: 497-505
104 **Patterson DM**, Padhani AR, Collins DJ. Technology insight: water diffusion MRI--a potential new biomarker of response to cancer therapy. *Nat Clin Pract Oncol* 2008; **5**: 220-233
105 **Le Bihan D**, Mangin JF, Poupon C, Clark CA, Pappata S, Molko N, Chabriat H. Diffusion tensor imaging: concepts and applications. *J Magn Reson Imaging* 2001; **13**: 534-546
106 **Provenzale JM**, Engelter ST, Petrella JR, Smith JS, MacFall JR. Use of MR exponential diffusion-weighted images to eradicate T2 "shine-through" effect. *AJR Am J Roentgenol* 1999; **172**: 537-539
107 **Thoeny HC**, De Keyzer F, Chen F, Ni Y, Landuyt W, Verbeken EK, Bosmans H, Marchal G, Hermans R. Diffusion-weighted MR imaging in monitoring the effect of a vascular targeting agent on rhabdomyosarcoma in rats. *Radiology* 2005; **234**: 756-764
108 **Mulkern RV**, Gudbjartsson H, Westin CF, Zengingonul HP, Gartner W, Guttmann CR, Robertson RL, Kyriakos W, Schwartz R, Holtzman D, Jolesz FA, Maier SE. Multi-component apparent diffusion coefficients in human brain. *NMR Biomed* 1999; **12**: 51-62
109 **Yamada I**, Aung W, Himeno Y, Nakagawa T, Shibuya H. Diffusion coefficients in abdominal organs and hepatic lesions: evaluation with intravoxel incoherent motion echo-planar MR imaging. *Radiology* 1999; **210**: 617-623
110 **Sun X**, Wang H, Chen F, De Keyzer F, Yu J, Jiang Y, Feng Y, Li J, Marchal G, Ni Y. Diffusion-weighted MRI of hepatic tumor in rats: comparison between in vivo and postmortem imaging acquisitions. *J Magn Reson Imaging* 2009; **29**: 621-628
111 **Bennett KM**, Schmainda KM, Bennett RT, Rowe DB, Lu H, Hyde JS. Characterization of continuously distributed cortical water diffusion rates with a stretched-exponential model. *Magn Reson Med* 2003; **50**: 727-734
112 **Parikh T**, Drew SJ, Lee VS, Wong S, Hecht EM, Babb JS, Taouli B. Focal liver lesion detection and characterization with diffusion-weighted MR imaging: comparison with standard breath-hold T2-weighted imaging. *Radiology* 2008; **246**: 812-822
113 **van den Bos IC**, Hussain SM, Krestin GP, Wielopolski PA. Liver imaging at 3.0 T: diffusion-induced black-blood echo-planar imaging with large anatomic volumetric coverage as an alternative for specific absorption rate-intensive echo-train spin-echo sequences: feasibility study. *Radiology* 2008; **248**: 264-271
114 **Takahara T**, Imai Y, Yamashita T, Yasuda S, Nasu S, Van Cauteren M. Diffusion weighted whole body imaging with background body signal suppression (DWIBS): technical improvement using free breathing, STIR and high resolution 3D display. *Radiat Med* 2004; **22**: 275-282
115 **DeVries AF**, Kremser C, Hein PA, Griebel J, Krezcy A, Ofner D, Pfeiffer KP, Lukas P, Judmaier W. Tumor microcirculation and diffusion predict therapy outcome for primary rectal carcinoma. *Int J Radiat Oncol Biol Phys* 2003; **56**: 958-965
116 **Pope WB**, Kim HJ, Huo J, Alger J, Brown MS, Gjertson D, Sai V, Young JR, Tekchandani L, Cloughesy T, Mischel PS, Lai A, Nghiemphu P, Rahmanuddin S, Goldin J. Recurrent glioblastoma multiforme: ADC histogram analysis predicts response to bevacizumab treatment. *Radiology* 2009; **252**: 182-189
117 **Moffat BA**, Chenevert TL, Lawrence TS, Meyer CR, Johnson TD, Dong Q, Tsien C, Mukherji S, Quint DJ, Gebarski SS, Robertson PL, Junck LR, Rehemtulla A, Ross BD. Functional diffusion map: a noninvasive MRI biomarker for early stratification of clinical brain tumor response. *Proc Natl Acad Sci USA* 2005; **102**: 5524-5529
118 **Fiebach JB**, Jansen O, Schellinger PD, Heiland S, Hacke W, Sartor K. Serial analysis of the apparent diffusion coefficient time course in human stroke. *Neuroradiology* 2002; **44**: 294-298
119 **Koh DM**, Blackledge M, Collins DJ, Padhani AR, Wallace T, Wilton B, Taylor NJ, Stirling JJ, Sinha R, Walicke P, Leach MO, Judson I, Nathan P. Reproducibility and changes in the apparent diffusion coefficients of solid tumours treated with combretastatin A4 phosphate and bevacizumab in a two-centre phase I clinical trial. *Eur Radiol* 2009; **19**: 2728-2738
120 **Cui Y**, Zhang XP, Sun YS, Tang L, Shen L. Apparent diffusion coefficient: potential imaging biomarker for prediction and early detection of response to chemotherapy in hepatic metastases. *Radiology* 2008; **248**: 894-900
121 **Harry VN**, Semple SI, Parkin DE, Gilbert FJ. Use of new imaging techniques to predict tumour response to therapy. *Lancet Oncol* 2010; **11**: 92-102
122 **Perini R**, Choe R, Yodh AG, Sehgal C, Divgi CR, Rosen MA. Non-invasive assessment of tumor neovasculature: techniques and clinical applications. *Cancer Metastasis Rev* 2008; **27**: 615-630
123 **Geraldes CF**, Laurent S. Classification and basic properties of contrast agents for magnetic resonance imaging. *Contrast Media Mol Imaging* 2009; **4**: 1-23
124 **Collins DJ**, Padhani AR. Dynamic magnetic resonance imaging of tumor perfusion. Approaches and biomedical challenges. *IEEE Eng Med Biol Mag* 2004; **23**: 65-83
125 **Reimer P**, Schuierer G, Balzer T, Peters PE. Application of a superparamagnetic iron oxide (Resovist) for MR imaging of human cerebral blood volume. *Magn Reson Med* 1995; **34**: 694-697
126 **Wintermark M**, Sesay M, Barbier E, Borbély K, Dillon WP, Eastwood JD, Glenn TC, Grandin CB, Pedraza S, Soustiel JF, Nariai T, Zaharchuk G, Caillé JM, Dousset V, Yonas H. Comparative overview of brain perfusion imaging techniques. *Stroke* 2005; **36**: e83-e99
127 **Yankeelov TE**, Gore JC. Dynamic Contrast Enhanced Magnetic Resonance Imaging in Oncology: Theory, Data Acquisition, Analysis, and Examples. *Curr Med Imaging Rev* 2009; **3**: 91-107
128 **Padhani AR**, Khan AA. Diffusion-weighted (DW) and dynamic contrast-enhanced (DCE) magnetic resonance imaging (MRI) for monitoring anticancer therapy. *Target Oncol* 2010; **5**: 39-52
129 **Weisskoff RM**, Chesler D, Boxerman JL, Rosen BR. Pitfalls in MR measurement of tissue blood flow with intravascular tracers: which mean transit time? *Magn Reson Med* 1993; **29**: 553-558
130 **Jackson A**, Buckley D, Parker G. Dynamic contrast-enhanced magnetic resonance imaging in oncology. 1st ed. New York: Springer Berlin Heidelberg, 2005
131 **Ostergaard L**, Sorensen AG, Kwong KK, Weisskoff RM,

Gyldensted C, Rosen BR. High resolution measurement of cerebral blood flow using intravascular tracer bolus passages. Part II: Experimental comparison and preliminary results. *Magn Reson Med* 1996; **36**: 726-736
132 **Vonken EP**, van Osch MJ, Bakker CJ, Viergever MA. Simultaneous quantitative cerebral perfusion and Gd-DTPA extravasation measurement with dual-echo dynamic susceptibility contrast MRI. *Magn Reson Med* 2000; **43**: 820-827
133 **Padhani AR**. MRI for assessing antivascular cancer treatments. *Br J Radiol* 2003; **76** Spec No 1: S60-S80
134 **Kassner A**, Annesley DJ, Zhu XP, Li KL, Kamaly-Asl ID, Watson Y, Jackson A. Abnormalities of the contrast re-circulation phase in cerebral tumors demonstrated using dynamic susceptibility contrast-enhanced imaging: a possible marker of vascular tortuosity. *J Magn Reson Imaging* 2000; **11**: 103-113
135 **Barbier EL**, Lamalle L, Décorps M. Methodology of brain perfusion imaging. *J Magn Reson Imaging* 2001; **13**: 496-520
136 **Tofts PS**, Berkowitz BA. Rapid measurement of capillary permeability using the early part of the dynamic Gd-DTPA MRI enhancement curve. *J Magn Reson* 1993; **102**: 129-136
137 **McIntyre DJ**, Robinson SP, Howe FA, Griffiths JR, Ryan AJ, Blakey DC, Peers IS, Waterton JC. Single dose of the antivascular agent, ZD6126 (N-acetylcolchinol-O-phosphate), reduces perfusion for at least 96 hours in the GH3 prolactinoma rat tumor model. *Neoplasia* 2004; **6**: 150-157
138 **Walker-Samuel S**, Parker CC, Leach MO, Collins DJ. Reproducibility of reference tissue quantification of dynamic contrast-enhanced data: comparison with a fixed vascular input function. *Phys Med Biol* 2007; **52**: 75-89
139 **Jackson A**. Analysis of dynamic contrast enhanced MRI. *Br J Radiol* 2004; **77** Spec No 2: S154-S166
140 **Tofts PS**, Brix G, Buckley DL, Evelhoch JL, Henderson E, Knopp MV, Larsson HB, Lee TY, Mayr NA, Parker GJ, Port RE, Taylor J, Weisskoff RM. Estimating kinetic parameters from dynamic contrast-enhanced T(1)-weighted MRI of a diffusable tracer: standardized quantities and symbols. *J Magn Reson Imaging* 1999; **10**: 223-232
141 **Larsson HB**, Tofts PS. Measurement of blood-brain barrier permeability using dynamic Gd-DTPA scanning--a comparison of methods. *Magn Reson Med* 1992; **24**: 174-176
142 **Buckley DL**. Uncertainty in the analysis of tracer kinetics using dynamic contrast-enhanced T1-weighted MRI. *Magn Reson Med* 2002; **47**: 601-606
143 **Siemann DW**, Horsman MR. Vascular targeted therapies in oncology. *Cell Tissue Res* 2009; **335**: 241-248
144 **Jackson A**, O'Connor JP, Parker GJ, Jayson GC. Imaging tumor vascular heterogeneity and angiogenesis using dynamic contrast-enhanced magnetic resonance imaging. *Clin Cancer Res* 2007; **13**: 3449-3459
145 **Salmon BA**, Siemann DW. Characterizing the tumor response to treatment with combretastatin A4 phosphate. *Int J Radiat Oncol Biol Phys* 2007; **68**: 211-217
146 **Evelhoch JL**, LoRusso PM, He Z, DelProposto Z, Polin L, Corbett TH, Langmuir P, Wheeler C, Stone A, Leadbetter J, Ryan AJ, Blakey DC, Waterton JC. Magnetic resonance imaging measurements of the response of murine and human tumors to the vascular-targeting agent ZD6126. *Clin Cancer Res* 2004; **10**: 3650-3657
147 **McKeage MJ**, Fong P, Jeffery M, Baguley BC, Kestell P, Ravic M, Jameson MB. 5,6-Dimethylxanthenone-4-acetic acid in the treatment of refractory tumors: a phase I safety study of a vascular disrupting agent. *Clin Cancer Res* 2006; **12**: 1776-1784
148 **Buonaccorsi GA**, Roberts C, Cheung S, Watson Y, O'Connor JP, Davies K, Jackson A, Jayson GC, Parker GJ. Comparison of the performance of tracer kinetic model-driven registration for dynamic contrast enhanced MRI using different models of contrast enhancement. *Acad Radiol* 2006; **13**: 1112-1123
149 **Salmon HW**, Siemann DW. Effect of the second-generation vascular disrupting agent OXi4503 on tumor vascularity. *Clin Cancer Res* 2006; **12**: 4090-4094
150 **Nico B**, Benagiano V, Mangieri D, Maruotti N, Vacca A, Ribatti D. Evaluation of microvascular density in tumors: pro and contra. *Histol Histopathol* 2008; **23**: 601-607
151 **Gaya A**, Daley F, Taylor NJ, Tozer G, Qureshi U, Padhani A, Pedley RB, Begent R, Wellsted D, Stirling JJ, Rustin G. Relationship between human tumour angiogenic profile and combretastatin-induced vascular shutdown: an exploratory study. *Br J Cancer* 2008; **99**: 321-326
152 **Tozer GM**. Measuring tumour vascular response to antivascular and antiangiogenic drugs. *Br J Radiol* 2003; **76** Spec No 1: S23-S35
153 **Dalal S**, Burchill SA. Preclinical evaluation of vascular-disrupting agents in Ewing's sarcoma family of tumours. *Eur J Cancer* 2009; **45**: 713-722
154 **McPhail LD**, Griffiths JR, Robinson SP. Assessment of tumor response to the vascular disrupting agents 5,6-dimethylxanthenone-4-acetic acid or combretastatin-A4-phosphate by intrinsic susceptibility magnetic resonance imaging. *Int J Radiat Oncol Biol Phys* 2007; **69**: 1238-1245
155 **Zhao D**, Richer E, Antich PP, Mason RP. Antivascular effects of combretastatin A4 phosphate in breast cancer xenograft assessed using dynamic bioluminescence imaging and confirmed by MRI. *FASEB J* 2008; **22**: 2445-2451
156 **Maxwell RJ**, Wilson J, Prise VE, Vojnovic B, Rustin GJ, Lodge MA, Tozer GM. Evaluation of the anti-vascular effects of combretastatin in rodent tumours by dynamic contrast enhanced MRI. *NMR Biomed* 2002; **15**: 89-98
157 **van der Sanden BP**, Rozijn TH, Rijken PF, Peters HP, Heerschap A, van der Kogel AJ, Bovée WM. Noninvasive assessment of the functional neovasculature in 9L-glioma growing in rat brain by dynamic 1H magnetic resonance imaging of gadolinium uptake. *J Cereb Blood Flow Metab* 2000; **20**: 861-870
158 **de Langen AJ**, van den Boogaart VE, Marcus JT, Lubberink M. Use of H2(15)O-PET and DCE-MRI to measure tumor blood flow. *Oncologist* 2008; **13**: 631-644
159 **Niermann KJ**, Fleischer AC, Huamani J, Yankeelov TE, Kim DW, Wilson WD, Hallahan DE. Measuring tumor perfusion in control and treated murine tumors: correlation of microbubble contrast-enhanced sonography to dynamic contrast-enhanced magnetic resonance imaging and fluorodeoxyglucose positron emission tomography. *J Ultrasound Med* 2007; **26**: 749-756
160 **Padhani AR**, Miles KA. Multiparametric imaging of tumor response to therapy. *Radiology* 2010; **256**: 348-364

S- Editor Cheng JX **L- Editor** Kerr C **E- Editor** Zheng XM